JOURNAL OF CATALYSIS 85, 477–487 (1984)

Kinetics of Vapor-Phase Electrochemical Oxidative Dehydrogenation of Ethylbenzene

JAMES N. MICHAELS[1] AND COSTAS G. VAYENAS[2]

Department of Chemical Engineering, Massachusetts Institute of Technology, Cambridge, Massachusetts 02139

Received June 1, 1983; revised August 18, 1983

The vapor-phase electrochemical oxidative dehydrogenation of ethylbenzene to styrene was studied at 575°C and atmospheric pressure on a polycrystalline platinum electrocatalyst in a stabilized zirconia electrochemical reactor. Electrochemical supply of oxygen to the electrocatalytic surface increases both the dehydrogenation rate and the deep oxidation rate. Carbon dioxide formation is oxygen-limited and its rate is linear in current density. The dehydrogenation rate is enhanced as much as 600% by moderate current densities; this electrocatalytic enhancement reaches an ethylbenzene-concentration-dependent asymptote at larger current densities. Addition of gas-phase hydrogen suppresses both the deep oxidation rate and the current-induced increase of the dehydrogenation rate. A two-site Langmuir–Hinshelwood type reaction mechanism is proposed which quantitatively describes these results. In this model, the electrocatalytic enhancement of the dehydrogenation rate results from a surface oxidative dehydrogenation step in which adsorbed ethylbenzene reacts with oxidized surface sites to form styrene and water.

I. INTRODUCTION

Styrene, ranked 22nd on the list of top volume chemicals produced in the United States (*1*), is produced by the catalytic vapor-phase dehydrogenation of ethylbenzene. This reaction is endothermic and equilibrium limited; at 600°C, the equilibrium constant is 0.19 (*2*), and the typical industrial per-pass conversion of ethylbenzene is 55–60% (*3*). Because the ethylbenzene–styrene separation is difficult and expensive (*4*), alternative processes have been sought which increase the per-pass yield of styrene. Oxidative dehydrogenation, in which product hydrogen is selectively removed from the reaction mixture by reaction with a suitable oxidant such as oxygen or SO_2 has been widely studied (*5–11*). A second alternative is coproduction of styrene and propylene oxide via the Oxirane process.

This work is part of an investigation of a third alternative, the electrochemical oxidative dehydrogenation of ethylbenzene to styrene. In this process, ethylbenzene is fed as a "fuel" to a high-temperature, solid-electrolyte fuel cell, shown schematically in Fig. 1. The cell is constructed by depositing porous electrodes on two sides of an impermeable, oxygen-ion conducting solid electrolyte. Oxygen adsorbs dissociatively and is reduced at the air-side electrode. When an electrical current is drawn in the external circuit, oxygen ions migrate through the electrolyte to the fuel-side electrode where (ideally) they react with ethylbenzene to form styrene and water. The overall reaction in this cell is the oxidative dehydrogenation of ethylbenzene with oxygen.

This electrochemical process offers a number of advantages over the conventional catalytic methods. First, this system can be used to directly and efficiently cogenerate electricity (*13*). Second, the electrochemical process allows one to increase

[1] Present address: Department of Chemical Engineering, University of California, Berkeley, California.

[2] Present address: Department of Chemical Engineering, University of Patras, Patras, Greece.

0021-9517/84 $3.00

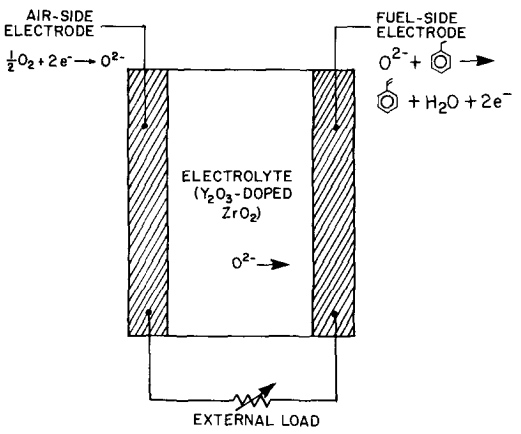

FIG. 1. Schematic of ethylbenzene solid-electrolyte fuel cell. See text for details.

the per-pass styrene yield without adding oxygen to ethylbenzene in the gas phase, thereby diminishing flammability or explosion hazards and allowing operation at significantly higher ethylbenzene concentrations. Third, the control of an electrochemical reactor is simplified, as the reaction rate and thermal energy generation rate are controlled primarily by the external electrical current.

The inherent complexity and expense of solid-state electrochemical reactors places particularly stringent demands on their chemical selectivity and electrical efficiency in order to compete favorably with conventional reactors. Of primary importance is the choice of an electrochemically active and selective fuel-side electrode. This report discusses the selectivity of polycrystalline platinum electrodes for styrene production and concentrates on the kinetics of ethylbenzene dehydrogenation and oxidation to CO_2. The electrical behavior of these electrodes is discussed elsewhere (*14, 16*).

II. EXPERIMENTAL

Kinetic studies were made with the electrochemical reactor shown in Fig. 2. This reactor was constructed from a 46-cm-long, 1.9-cm-o.d., 1.6-cm-i.d. 8 w/o yttria-stabilized zirconia tube (Zircoa Products). Platinum air-side and fuel-side electrodes were deposited on the center 10 cm of the outside and inside tube surfaces, respectively. These electrodes were made by painting the cleaned tube surfaces with Engelhard A-3788 fluxed platinum ink and calcining in air at 850°C. The superficial area of the fuel-side electrode was 49.9 cm^2. The specific surface area of this electrode was estimated to be 300 cm^2/cm^2 of superficial area (*15*). The active volume of the re-

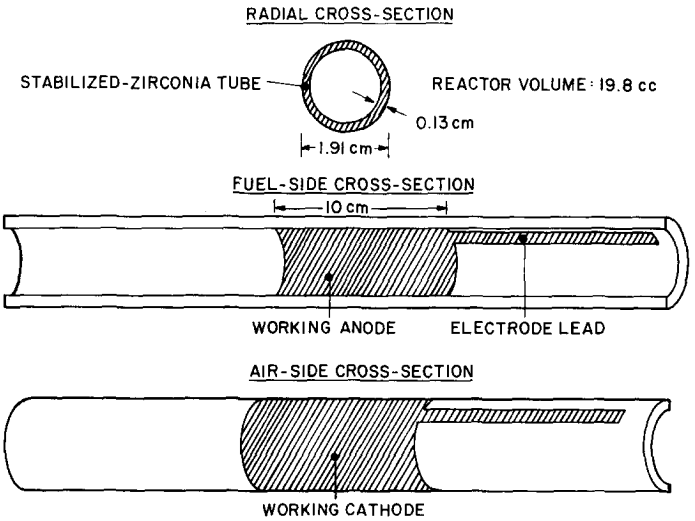

FIG. 2. Tubular zirconia-electrolyte electrochemical reactor with porous platinum electrodes.

actor, the volume enclosed by the fuel-side electrode, was 19.3 cm^3. Details of construction of this reactor are given elsewhere (*16*).

The reactor was placed into a 3-cm-diameter tubular furnace and sealed into the flow system shown in Fig. 3 with CAJON ULTRATORR vacuum fittings. Helium was saturated with ethylbenzene by sparging through a thermostatted column of liquid ethylbenzene, and the reactor feedstream composition was controlled by addition of make-up helium, hydrogen, or oxygen. Reactor feed and effluent streams were sampled for on-line gas chromatographic analysis by proper adjustment of 6-port selector and gas-sampling valves. The feed stream could be diverted from the reactor or the reactor isolated by adjustment of three shutoff valves. The total noncondensible flowrates of the feed and product streams were measured with a bubble flowmeter. All connecting tubing was 0.32- or 0.64-cm-o.d. Type 316 stainless steel. Gas lines and valves were heated to prevent adsorption or condensation of high-boiling compounds.

Chemical analyses were performed with a Hewlett–Packard Model 5730A gas chromatograph with a thermal conductivity detector. Two columns were required. A 183 × 0.32-cm stainless-steel column packed with 60/80 mesh 5% SP-1200/1.75% Bentone-34 on Supelcoport separated aromatics and aliphatics. A 91 × 0.32-cm 60/80 mesh Carbosieve S column separated the fixed gases. Peaks were recorded and integrated with a Hewlett–Packard Model 3380S digital integrator.

The electrochemical cell was driven galvanostatically with an AMEL Model 549 potentiostat/galvanostat. The reactor working voltage and current were measured with Fluke Model 8600A digital multimeters.

In a typical experiment, the feed stream flowrate and composition, reactor temperature, and electrical current were adjusted, and the cell voltage was monitored until it stabilized at its steady-state value. The working voltage, current, and chemical composition of the feed and product streams were then measured. During the approach to steady state, the flowrate of noncondensibles in the feed was measured to determine the residence time of the reactor. All results discussed below are steady-state results.

The reactor was operated as a differential

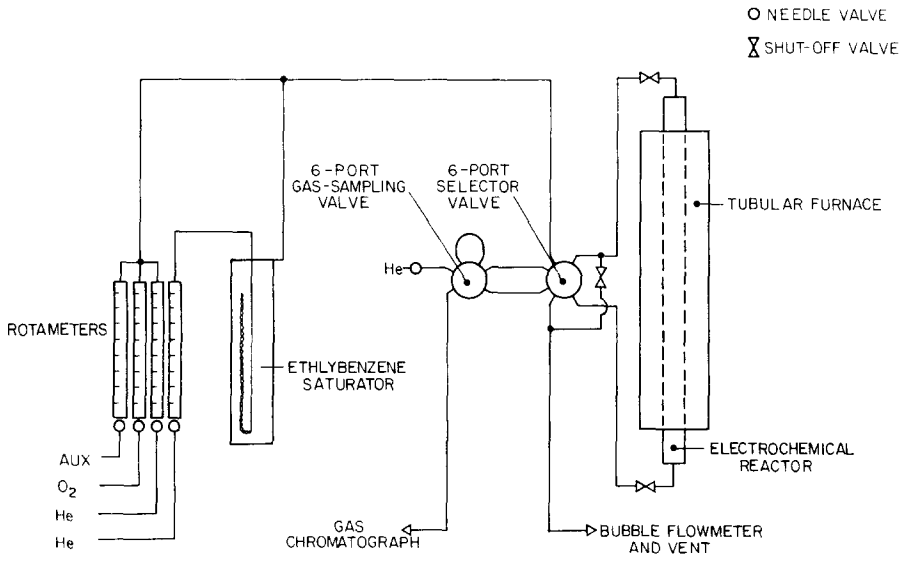

FIG. 3. Experimental flow system.

reactor (with respect to ethylbenzene conversion) in all measurements; ethylbenzene conversion did not exceed 15%. Reaction rates, therefore, were calculated from the flowrates of the products directly. Rates, rate constants, and current density are normalized by the area of active electrolyte.

The only detectable products were H_2, CO, CO_2, water, methane, ethylene, benzene, toluene, and styrene. Carbon atom balance nonclosure did not exceed ±2% and showed no consistent loss of material. No significant formation of other oxygenated species or coking of the catalyst was detected.

III. RESULTS

The pure ionic conductivity of the solid electrolyte was verified by flowing helium–oxygen mixtures of known composition through the electrochemical reactor and measuring the open-circuit voltage. Measured voltages were typically within ±2 mV of those predicted by the Nernst equation:

$$E_0 = (RT/4F)\ln(0.21/p_{O_2}) \qquad (1)$$

in which F is the Faraday constant, p_{O_2} is the oxygen pressure at the fuel-side electrode, and 0.21 atm is the prevailing partial pressure at the air-side electrode.

It is convenient to lump the production of CO and CO_2 and that of benzene and toluene in the analysis of the chemical rate data. CO plus CO_2 formation is termed "deep oxidation," and benzene plus toluene formation is designated "dealkylation."

Figure 4 shows the effect of electrochemically pumping oxygen to the fuel-side electrode on the steady-state dehydrogenation (r_{DH}), deep oxidation (r_{DO}), dealkylation (r_{DA}), and overall (r_T) rates with varying current density (i) between 0 and 60 A/m² at 575°C. When the cell is open-circuited (i = 0 A/m²), the fuel-side electrode acts as a conventional dehydrogenation catalyst with a selectivity to styrene of 78%. The major byproducts are benzene and toluene with corresponding amounts of ethylene

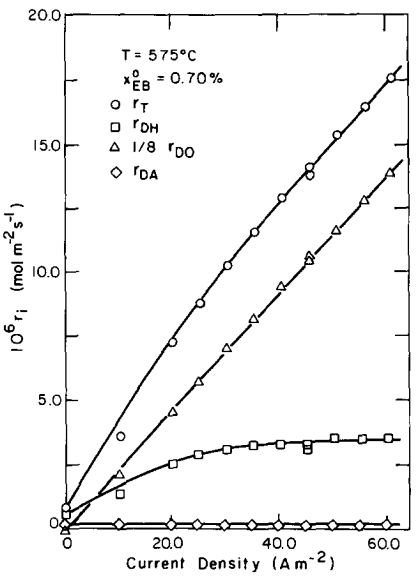

FIG. 4. Current dependence of total rate and rates of product formation, platinum electrode, T = 575°C, feed ethylbenzene mole fraction = 0.70%. Deep oxidation rate plotted as moles *ethylbenzene* converted to CO_2.

and methane. The predominant electrochemical products are CO and CO_2. Surprisingly, the dehydrogenation rate is strongly current dependent. The dealkylation rate is essentially current independent and accounts for less than 5% of overall reaction rate at most current densities.

A more detailed investigation of the current dependence of the dehydrogenation rate is shown in Fig. 5. At low feed ethylbenzene concentrations, moderate current densities increase the styrene rate as much as 600%. The electrocatalytic effect saturates at large current densities and low ethylbenzene mole fractions. This effect cannot be ascribed to a shift in the dehydrogenation equilibrium, as the equilibrium conversion of ethylbenzene is 80% or larger under these conditions (*2*), and the measured conversion did not exceed 15%.

As shown in Fig. 6, the dehydrogenation rate is first order in ethylbenzene mole fraction at zero current; the first-order rate constant is 9.65×10^{-5} mol/m² s. The rate be-

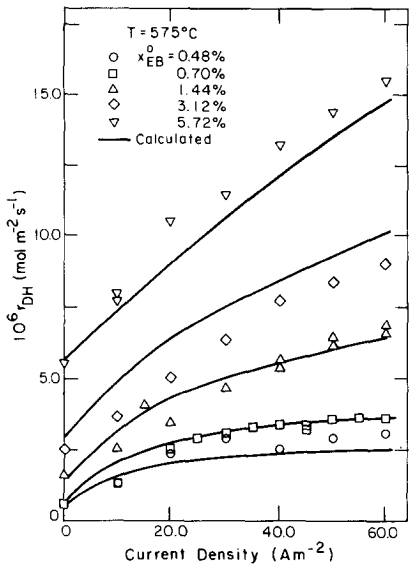

FIG. 5. Current dependence of dehydrogenation rate, platinum electrode, T = 575°C. Parameter: feed ethylbenzene mole fraction.

comes less-than-first-order at finite current densities.

The dealkylation rate, as mentioned above, is independent of current density. it is also first order in ethylbenzene with rate constant 3.03×10^{-5} mol/m^2 s.

The deep oxidation rate, shown in Fig. 7, is linear in current density with slope 1.84×10^{-6} mol/C and zero order in ethylbenzene. The CO_2 : CO ratio is large at all nonzero current densities and ethylbenzene concentrations. Carbon and oxygen atom balances indicate that the hydrocarbons are deeply oxidized completely to CO or CO_2 and water.

The dehydrogenation and deep oxidation rates are strongly inhibited by gas-phase hydrogen as shown by Figs. 8 and 9. At large hydrogen mole fractions, the dehydrogenation rate is depressed to its value at open circuit. CO and CO_2 formation are more deeply inhibited by hydrogen; at a fixed current density, the deep oxidation rate decreases sharply with increasing hydrogen concentration, approaching zero at very large mole fractions.

Finally, Figs. 10 and 11 show the effect of adding oxygen to the reactor feed at open circuit. Both the dehydrogenation rate and the deep oxidation rate increase with increasing oxygen partial pressure. This effect is qualitatively similar to the effect of increasing current density seen in Figs. 5 and 7.

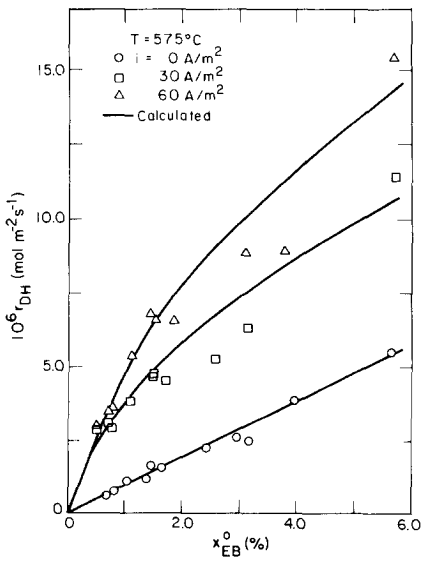

FIG. 6. Ethylbenzene concentration dependence of dehydrogenation rate, platinum electrode, T = 575°C. Parameter: current density.

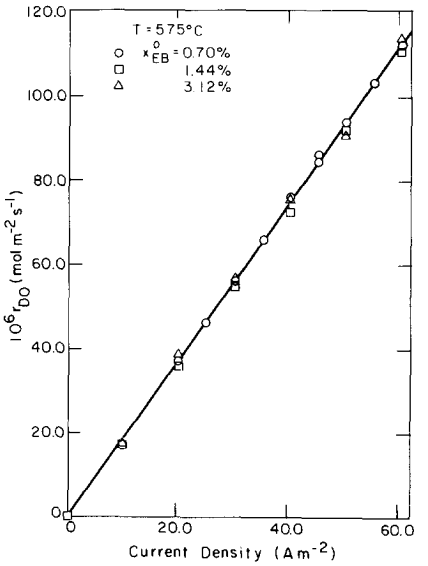

FIG. 7. Current dependence of deep oxidation rate, platinum electrode, T = 575°C. Parameter: feed ethylbenzene mole fraction.

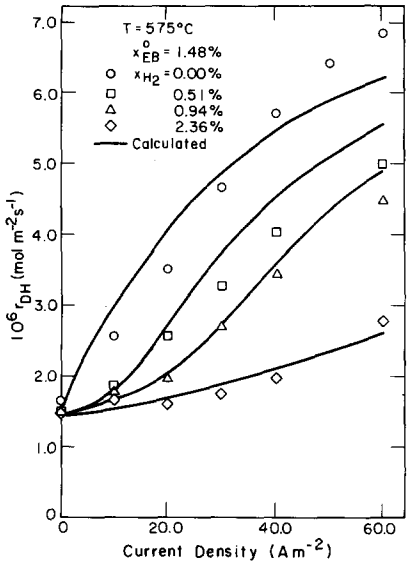

FIG. 8. Effect of gas-phase hydrogen on the dehydrogenation rate, platinum electrode, T = 575°C, feed ethylbenzene mole fraction = 1.48%. Parameter: feed hydrogen mole fraction.

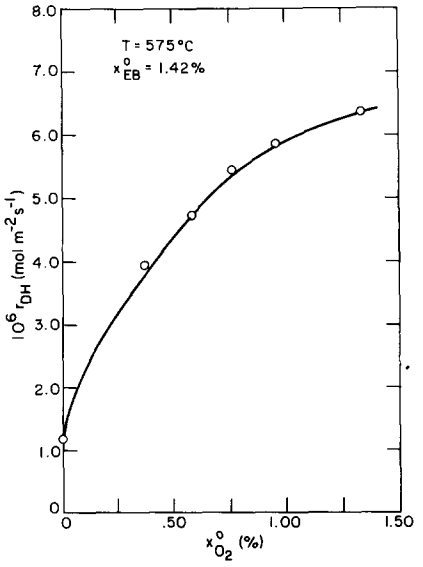

FIG. 10. Oxygen concentration dependence of dehydrogenation rate at open circuit, platinum electrode, T = 575°C, feed ethylbenzene mole fraction = 1.42%.

IV. DISCUSSION

The utility of platinum as an electrocatalyst for electrooxidative dehydrogenation of ethylbenzene is severely limited by its activity for deep oxidation. Despite this technical disappointment, these results do raise some interesting points about the ac-

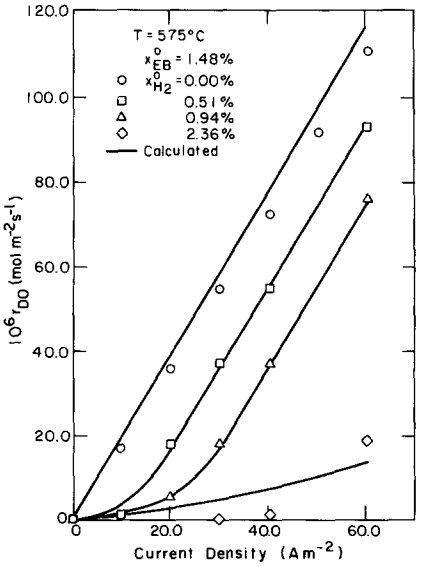

FIG. 9. Effect of gas-phase hydrogen on the deep oxidation rate, platinum electrode, T = 575°C, feed ethylbenzene mole fraction = 1.48%. Parameter: feed hydrogen mole fraction.

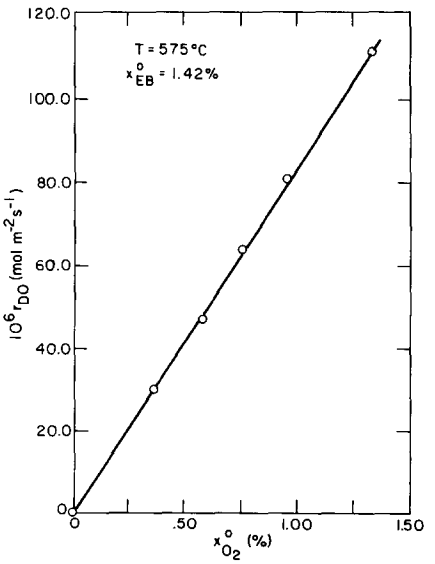

FIG. 11. Oxygen concentration dependence of deep oxidation rate at open circuit, platinum electrode, T = 575°C, feed ethylbenzene mole fraction = 1.42%.

tivity and selectivity of platinum for ethylbenzene dehydrogenation and oxidation. This is discussed below, with particular emphasis on the electrochemical enhancement of the dehydrogenation rate and the marked, selective inhibitory effect of gas-phase hydrogen.

The platinum electrocatalyst showed no apparent loss of catalytic activity during experimentation, and no evidence exists of coke formation or other type of catalyst poisoning. The consistent closure of the carbon-atom balance indicates that all major products were detected and properly quantified.

The primary source of CO and CO_2 is deep oxidation of ethylbenzene. The current independence of the dealkylation rate indicates that neither benzene nor toluene are oxidized, as deep oxidation would cause the dealkylation rate to decrease as current increases. For the same reason, the current dependence of the dehydrogenation rate suggests that styrene, too, is not attacked by oxygen to a significant extent. The absence of these sequential reactions most likely results from the difference between product and reactant concentrations at the small total conversions in this study.

On the basis of these observations, the system is well described by the reaction network:

$$C_8H_{10} \rightarrow C_8H_8 + H_2 \quad (2)$$

$$C_8H_{10} + H_2 \rightarrow C_7H_8 + CH_4 \quad (3)$$

$$C_8H_{10} \rightarrow C_6H_6 + CH_2CH_2 \quad (4)$$

$$C_8H_{10} + \tfrac{21}{2}\,O_2 \rightarrow 8\,CO_2 + 5\,H_2O \quad (5)$$

$$C_8H_{10} + \tfrac{13}{2}\,O_2 \rightarrow 8\,CO + 5\,H_2O \quad (6)$$

$$CO + \tfrac{1}{2}\,O_2 \rightarrow CO_2 \quad (7)$$

$$H_2 + \tfrac{1}{2}\,O_2 \rightarrow H_2O \quad (8)$$

It would seem natural to express the deep oxidation and oxidative dehydrogenation of ethylbenzene as reactions between ethylbenzene and oxygen ions on the platinum electrode surface. However, the electrical behavior of the electrode suggests that oxygen alone is involved in the dominant charge-transfer reaction (*16*). This suggests strongly that ethylbenzene, hydrogen, and CO react with *neutral* oxygen adatoms in purely catalytic reactions. Varying the current density does no more than increase the supply of oxygen to the catalyst and is effectively equivalent to increasing the gas-phase partial pressure of oxygen. The qualitative similarity between the enhancement of the dehydrogenation rate induced by electrochemically supplied and gas-phase oxygen, shown by Figs. 5 and 10, further supports this conclusion.

The ethylbenzene-concentration independence of the deep oxidation rate indicates that formation of CO and CO_2 is oxygen limited. Measurement of the oxygen surface activity at open circuit by Solid Electrolyte Potentiometry (*12*) corroberates this: in the presence of 1.42 mol% ethylbenzene, the square of the surface activity, a_O^2, varied from 8.54×10^{-12} to 2.84×10^{-11} as the partial pressure of oxygen increased from 0.36 to 1.32 atm. If oxygen were in adsorption equilibrium, a_O^2 would equal the prevailing oxygen partial pressure (in atmospheres). The extreme depression of the oxygen activity below its equilibrium value suggests that the oxygen surface coverage is small and indicates that surface reactions with oxygen are strongly oxygen limited. Because the electrochemical oxygen flux to the catalyst surface is proportional to the current density, the linearity of the deep oxidation rate in current density is also a manifestation of this oxygen limitation.

The enhancement of the ethylbenzene dehydrogenation rate by oxygen is reminiscent of a similar enhancement of cyclohexane and cyclohexene dehydrogenation rates at low pressure on preoxidized platinum single crystals (*17, 18*). Three models, originally developed to describe enhanced bonding of H_2 and CO on preoxidized platinum surfaces (*20, 21*), have been proposed to explain this enhancement of the low-pressure dehydrogenation rates (*22*). The

first model assumes that surface or subsurface (*19*) oxide formation alters the electronic structure of the surface platinum atoms. This would effect the binding of hydrogen and the hydrocarbons, thereby altering catalytic activity and selectivity. The second model suggests that the strongly bound oxygen atoms are active in compound formation with other adsorbates; these oxygenated intermediates can provide an alternate pathway for dehydrogenation. The third model proposes that platinum surface oxidation results in reconstruction of the surface which would create new catalytically active sites. Of these models, the third is believed to be the least likely, as LEED showed little variation in the surface structure as a function of surface coverage (*20*).

The oxygen-induced enhancement of ethylbenzene dehydrogenation may also be caused by a similar mechanism. Of these three models, the second appears to describe the kinetics in the most reasonable way. This can be justified for two reasons. First, the platinum electrode was calcined in air at 850°C for approximately 1 h and was not reduced prior to use. Due to the observed stability of the oxide to reducing atmospheres below 1000 K (*20*), it is likely that the platinum surface was fully oxidized during all measurements. Further addition of oxygen, therefore, should not have increased the amount nor electronic effect of the surface oxide. Second, because of the high hydrocarbon pressures and extremely small oxygen surface activities of this study, it is likely that the platinum surface was covered by a carbonaceous overlayer at steady state. These submonolayer carbon layers have been observed to form on clean (*24*) and oxidized (*23*) platinum single-crystal surfaces during high-pressure hydrocarbon catalysis. This overlayer eliminates the structure sensitivity of cyclohexene and cyclohexane dehydrogenation (*24*), and could attenuate the catalytic effects of platinum surface oxidation. This latter point is supported by the independence of the cyclohexane dehydrogenation rate to preoxidation of the platinum surface at atmospheric pressure (*23*).

The enhancement of the ethylbenzene rate, and all important experimental observations in general, can be explained by postulating that chemisorbed oxygen reacts with the carbonaceous overlayer on the surface to form oxidized sites. Adsorbed ethylbenzene subsequently reacts with these sites to form styrene and water directly. Because the coverage of oxidized sites varies with the supply of oxygen to the surface, the dehydrogenation rate is current- and oxygen-concentration dependent. Adsorbed oxygen also reacts with adsorbed hydrogen and ethylbenzene directly to form CO_2 and water.

The inhibitory effect of hydrogen is also explained naturally by this model. If its oxidation rate is suitably large, hydrogen effectively scavenges oxygen from the surface, reducing the deep oxidation rate and the number of oxidized sites on the surface. The latter effect reduces the dehydrogenation rate to its open-circuit value. It is improbable that hydrogen inhibition is due to simple blockage of catalytic sites by adsorbed hydrogen. The desorption temperature of hydrogen on clean (*18*) and oxidized (*20*) platinum surfaces is 400 K or less, much lower than the reaction temperature of 848 K in this study. Therefore, the hydrogen surface coverage should be quite small at all hydrogen partial pressures. Furthermore, if the inhibition were adsorption related, the *open-circuit* dehydrogenation rate would also be inhibited; this was not observed.

These ideas can be quantified by the following simple kinetic model. This model does not attempt to describe all of the reaction steps and intermediates involved in ethylbenzene dehydrogenation and deep oxidation. This would be a formidible task and is not justified by the extent of the data. Rather, emphasis is placed on developing the simplest model which captures the important aspects of the qualitative mecha-

nism described above and adequately describes the experimental observations. Details of the derivation are presented in (*14*). For simplicity, the dealkylation reactions are ignored due to their small contribution to the overall conversion of ethylbenzene. Deep oxidation of styrene and CO production are neglected for similar reasons. The discussion which follows is valid when gas-phase oxygen is absent. The model is easily generalized to account for nonelectrochemical supply of oxygen (*14*).

The catalytic surface is assumed to have two active sites, S_1 and S_2. Ethylbenzene and styrene are assumed to be in adsorption equilibrium with type 1 sites at suitably low coverages such that their isotherms are linear. This assumption appears to be justified by the low desorption temperature of benzene on clean and carbon-covered platinum surfaces (*22*). Hydrogen and oxygen adsorb dissociatively on the type 1 sites; hydrogen is assumed to be in adsorption equilibrium and at low coverage. As discussed above, oxygen is not in equilibrium. Adsorption of CO_2 and water should be negligibly small.

In the absence of gas-phase oxygen, oxygen atoms are supplied to type 1 sites at a rate equal to the oxygen ion flux to the electrode, $j_O = i/2F$:

$$O(a,C) + S_1 \xrightarrow{j_O} O(a) \qquad (9)$$

O(a,C) is dissociatively adsorbed oxygen adsorbed on the air-side electrode (cathode). The adsorbed oxygen takes part in three reactions. The first two are oxidation of adsorbed ethylbenzene and hydrogen to produce CO_2 and H_2O. It is assumed that the rate-determining step in each reaction is first order in the adsorbed reactants with the rate constants shown in

$$C_8H_{10}(a) + O(a) \xrightarrow{k_{DO}} 8CO_2(g) + 5H_2O(g) \qquad (10)$$

$$H(a) + O(a) \xrightarrow{k_{HO}} H_2O(g) \qquad (11)$$

The third reaction is oxidation of type 2 sites on the surface. It is assumed that surface oxidation is rapid at 575°C and that equilibrium between adsorbed oxygen and the oxidized surface is achieved at steady state. If the oxide has stoichiometry S_2O, this equilibrium is written

$$O(a) + S_2 \overset{K_*}{=} S_1 + S_2O \qquad (12)$$

where K_* is the oxidation equilibrium constant.

Finally, ethylbenzene dehydrogenation is assumed to occur by two parallel reactions. The first is a nonoxidative surface reaction whose rate-determining step is first order in adsorbed ethylbenzene:

$$C_8H_{10}(a) \xrightarrow{k_{DH}} C_8H_8(a) + 2H(a) \qquad (13)$$

The second is an oxidative reaction with oxidized sites:

$$C_8H_{10}(a) + S_2O \xrightarrow{k_*} C_8H_8(a) + H_2O(g) + S_2 \qquad (14)$$

k_{DH} and k_* are the rate constants of the nonoxidative and oxidative dehydrogenation rate-determining steps, respectively.

This simple mechanism yields the following expressions for the dehydrogenation and deep oxidation rates which are valid in the absence of gas-phase oxygen:

$$r_{DH} = k_1 x_{EB} + \frac{k_2 x_{EB} j_O}{x_{EB} + k_3 j_O + k_4 \sqrt{x_{H2}}} \qquad (15)$$

$$r_{DO} = \frac{8 x_{EB} j_O}{21(x_{EB} + k_4 \sqrt{x_{H2}})} \qquad (16)$$

where

$$k_1 = k_{DH} K_{EB} \qquad (17)$$

$$k_2 = k_* K_* / 21 k_{DO} \qquad (18)$$

$$k_3 = K_* / 21 k_{DO} K_{EB} \qquad (19)$$

$$k_4 = k_{HO} \sqrt{K_H} / 21 k_{DO} K_{EB} \qquad (20)$$

K_H and K_{EB} are the hydrogen and ethylbenzene adsorption equilibrium constants, respectively. The k_1 is the first-order dehydrogenation rate constant measured at open circuit:

$$k_1 = 9.65 \times 10^{-5} \text{ mol/m}^2 \text{ s}$$

k_2 through k_4 were calculated from the

closed-circuit dehydrogenation rate data using the POWELL nonlinear, multivariate least-squares algorithm. The best values are

$$k_2 = 3.94 \times 10^{-2} \text{ mol/m}^2 \text{ s}$$

$$k_3 = 67.7 \text{ s/mol}$$

$$k_4 = 1.33$$

Reaction rates calculated with Eqs. (15) and (16) are shown by the solid lines in Figs. 5, 6, 8, and 9. The agreement between the calculated and measured rates is quantitative in most instances. This agreement obviously does not constitute proof of the proposed mechanism. However, it does show that the surface oxidation model is capable of correctly describing the varied and complex behavior of this catalytic system.

V. CONCLUSIONS

The dehydrogenation and deep oxidation rates of ethylbenzene on a platinum electrocatalyst in a zirconia-electrolyte electrochemical reactor are both increased by electrochemical supply of oxygen to the catalytic surface. In the absence of significant amounts of hydrogen in the gas phase, the major product in such a reactor at moderate and large current densities is CO_2, with lesser amounts of styrene, benzene, and toluene.

Addition of hydrogen to the gas phase strongly inhibits deep oxidation and, to a lesser extent, dehydrogenation. The inhibition appears to result primarily from competitive oxidation of hydrogen and ethylbenzene on the platinum surface. An interesting practical result of this is that hydrogen can be *selectively* oxidized from a mixture of ethylbenzene, styrene, and hydrogen with little loss of the hydrocarbons to CO_2.

The kinetics of this electrochemical system are well described by a Langmuir–Hinshelwood type mechanism which assumes the existence of two types of sites on the platinum surface. The hydrocarbons, hydrogen, and oxygen adsorb and react on one type of site to form styrene, benzene, toluene, CO, and CO_2. Adsorbed oxygen also oxidizes the other type of site, and adsorbed ethylbenzene can react with these oxidized sites to form styrene and water. This oxidative dehydrogenation pathway is responsible for the observed electrocatalytic enhancement of the dehydrogenation rate.

Electrochemically supplied oxygen appears to behave identically to gas-phase oxygen. In the absence of significant amounts of gas-phase hydrogen, the net result of increasing the current or oxygen partial pressure is to produce CO_2 and reduce the selectivity to styrene. This loss in selectivity precludes the use of platinum electrodes for the production of styrene. However, the inhibition of the deep oxidation rate by hydrogen suggests a slightly different reactor configuration which should be more viable for styrene production. If the electrochemical reactor is packed with a commercial dehydrogenation catalyst, a hydrogen-rich ethylbenzene–styrene mixture will be produced at the platinum electrode. Hydrogen should be selectively oxidized from this mixture, thereby allowing power generation with little degradation in chemical selectivity. Furthermore, if the reaction mixture is near equilibrium, this selective hydrogen combustion would shift the equilibrium toward styrene. Such a hybrid reactor has been tested and the results will be published elsewhere.

We note that the present results are the first known application of a solid electrolyte reactor to enhance the rate of a dehydrogenation reaction and simultaneously produce electrical power.

APPENDIX: NOMENCLATURE

E_0	open-circuit cell voltage
F	Faraday constant
K_{EB}	ethylbenzene adsorption constant
K_H	hydrogen adsorption constant

K_* surface oxidation equilibrium constant
R gas constant
S_1 type 1 catalytic site
S_2 type 2 catalytic site
T absolute temperature
(a) adsorbed species
a_O oxygen atom surface activity
(g) gas-phase species
i current density
j_O oxygen atom flux to fuel-side electrode
k_{DH} dehydrogenation surface rate constant
k_{DO} deep oxidation surface rate constant
k_{HO} hydrogen oxidation surface rate constant
k_* oxidative-dehydrogenation surface rate constant
r_{DA} dealkylation rate
r_{DH} dehydrogenation rate
r_{DO} deep oxidation rate
r_T total rate
x_{EB} ethylbenzene gas-phase mole fraction
x_{H2} hydrogen gas-phase mole fraction
x_{O2} oxygen gas-phase mole fraction

Superscript
0 feed-stream condition

ACKNOWLEDGMENTS

The authors thank Professor James Wei for his contributions to this work. This project was supported by the United States Department of Energy Grant number DE-AC02-80ER10694.

REFERENCES

1. C+E News, **60**(18), 11, (1982).
2. Gutman, L., Westrum, E. F. Jr., and Pitzer, K. S., *J. Amer. Chem. Soc.* **95,** 1246 (1943).
3. Kaeding, W. W., *Catal. Rev.* **8**(2), 307 (1973).
4. "Kirk-Othmer Encyclopedia of Chemical Technology," Vol. 19, pp. 62–68. Wiley, New York, 1969.
5. Alkhazov, T. G., Lisovskii, A. E., Safarov, M. G., and Dadasheva, A. M., *Kinet. Katal.* **13**(2), 509 (1972).
6. Cortes, A., and Seoane, J. L., *J. Catal.* **34,** 7 (1974).
7. Dzuewieke, Z., and Makawski, A., *React. Kinet. Catal. Lett.* **13**(1), 51 (1980).
8. Fujimoto, K., and Kunugi, T., *Ind. Eng. Chem., Proc. Des. Dev.* **20,** 319 (1981).
9. Adams, C. R., and Jennings, T. L., *J. Catal.* **17,** 157 (1970).
10. Gaspar, N. J., Cohen, A. D., Vadekar, M., and Pasternak, I. S., *Canad. J. Chem. Eng.* **53,** 79 (1975).
11. Vadekar, M., Pasternak, I. S., and Gaspar, N. J., *Canad. J. Chem. Eng.* **52,** 788 (1974).
12. Stoukides, M., and Vayenas, C. G., *J. Catal.* **64,** 18–28 (1980).
13. Bokris, J. O'M., and Reddy, A. K. N., "Modern Electrochemistry," Vol. 2. Plenum, New York, 1977.
14. Michaels, J. N., Sc.D. thesis, MIT, Cambridge, 1983.
15. Farr, R. D., and Vayenas, C. G., *J. Electrochem. Soc.* **127,** 1478 (1980).
16. Michaels, J. N., and Vayenas, C. G., to be published.
17. Smith, C. E., Biberian, J. P., and Somorjai, G. A., *J. Catal.* **57,** 426–443 (1979).
18. Davis, S. M., and Somorjai, G. A., *Surf. Sci.* **91,** 73–91 (1980).
19. Niehus, H., and Comsa, G., *Surf. Sci.* **93,** L147–L150 (1980).
20. McCabe, R. W., and Schmidt, L. D., *Surf. Sci.* **60,** 85–98 (1976).
21. McCabe, R. W., and Schmidt, L. D., *Surf. Sci.* **65,** 189–209 (1977).
22. Somorjai, G. A., "Chemistry in Two Dimensions: Surfaces," Chap. 9. Cornell Univ. Press, Ithaca, N.Y., 1981.
23. Herz, R. K., Gillespie, W. D., Petersen, E. E., and Somorjai, G. A., *J. Catal.* **67,** 371–386 (1981).
24. Kesmodel, L. L., Dubois, L. H., and Somorjai, G. A., *J. Chem. Phys.* 2180 (1979).